Paediatrics Publications   Paediatrics Department

1-1-2011

Combination of complex-based and magnitude-based multiecho water-fat separation for accurate quantification of fat-fraction

Huanzhou Yu
GE Healthcare, United States

Ann Shimakawa
GE Healthcare, United States

Catherine D.G. Hines
University of Wisconsin-Madison

Charles A. McKenzie
Western University, cmcken@uwo.ca

Gavin Hamilton
University of California, San Diego

See next page for additional authors

Citation of this paper:

Yu, Huanzhou; Shimakawa, Ann; Hines, Catherine D.G.; McKenzie, Charles A.; Hamilton, Gavin; Sirlin, Claude B.; Brittain, Jean H.; and Reeder, Scott B., "Combination of complex-based and magnitude-based multiecho water-fat separation for accurate quantification of fat-fraction" (2011). *Paediatrics Publications*. 1719.
https://ir.lib.uwo.ca/paedpub/1719

Authors

Huanzhou Yu, Ann Shimakawa, Catherine D.G. Hines, Charles A. McKenzie, Gavin Hamilton, Claude B. Sirlin, Jean H. Brittain, and Scott B. Reeder

Combination of Complex-Based and Magnitude-Based Multiecho Water-Fat Separation for Accurate Quantification of Fat-Fraction

Huanzhou Yu,[1]* Ann Shimakawa,[1] Catherine D. G. Hines,[2,3] Charles A. McKenzie,[4–6] Gavin Hamilton,[7] Claude B. Sirlin,[7] Jean H. Brittain,[8] and Scott B. Reeder[2,3,9,10]

Multipoint water–fat separation techniques rely on different water–fat phase shifts generated at multiple echo times to decompose water and fat. Therefore, these methods require complex source images and allow unambiguous separation of water and fat signals. However, complex-based water–fat separation methods are sensitive to phase errors in the source images, which may lead to clinically important errors. An alternative approach to quantify fat is through "magnitude-based" methods that acquire multiecho magnitude images. Magnitude-based methods are insensitive to phase errors, but cannot estimate fat-fraction greater than 50%. In this work, we introduce a water–fat separation approach that combines the strengths of both complex and magnitude reconstruction algorithms. A magnitude-based reconstruction is applied after complex-based water–fat separation to removes the effect of phase errors. The results from the two reconstructions are then combined. We demonstrate that using this hybrid method, 0–100% fat-fraction can be estimated with improved accuracy at low fat-fractions. Magn Reson Med 66:199–206, 2011. © 2011 Wiley-Liss, Inc.

Key words: water–fat separation; IDEAL; eddy currents; water–fat ambiguity; magnitude-based water–fat separation; hepatic steatosis; fat quantification

The applications of multiecho chemical shift based water–fat separation techniques are continuously expanding, both for robust fat suppression in routine clinical scanning (1,2) and for quantitative fat imaging such as evaluation of hepatic steatosis (3–5) and vertebral bone marrow (6). These methods rely on the different water–fat phase shifts generated at multiple echo times to estimate the amplitude of static (polarizing) field (B_0) field map and water and fat content on a voxel by voxel basis. Therefore, these methods require complex source images. In addition to the phase information contained within the acquired signals, robust water–fat separation methods often use the a priori information that magnetic field inhomogeneities are smooth, allowing accurate and complete separation of water and fat (7–11). However, complex-based water–fat separation methods are sensitive to unexpected phase errors in the source images, such as those from eddy currents. Although the impact of these phase errors is small and acceptable for most qualitative applications, as we show below, such phase errors can be clinically meaningful for quantitative applications.

Alternatively, water–fat separation can be achieved using only the magnitude of the complex source signals (12,13), including the original 2-point "Dixon" method (14). These "magnitude-based" methods are insensitive to phase errors in the source images, because the phase information is discarded. However, because of the lack of phase information, these methods alone are unable to determine fat fraction [i.e., fat/(water + fat)] over a 50% range (13). Additional information can be used to help the identification of water and fat, such as using low resolution spectroscopy (15) and difference in T_1 (3,16) or T_2^* relaxation parameters (17), which require either additional data or a more complex model.

A clinically useful fat quantification technique must be both accurate and robust. The complex-based and magnitude-based methods have complementary strengths and weaknesses. In this work, we introduce a new water–fat separation approach that combines the strengths of both complex and magnitude reconstruction methods. A complex-based approach is used to separate the fat and water signals to achieve a dynamic range of 0–100% fat-fraction, followed by a magnitude-based reconstruction to fine tune the quantification and remove phase errors. The results from the two reconstructions are then combined to provide consistent noise performance for all water–fat combinations. Using this "hybrid" approach, reliable and accurate fat-fractions can be estimated, particularly at low fat-fractions.

THEORY

Figure 1 demonstrates the impact of eddy-current induced phase errors on quantitative water–fat separation applications. Figure 1a illustrates water and fat images reconstructed from a six-point multiecho abdominal scan and T_2^*-Iterative Decomposition of Water and

[1]Applied Science Laboratory, GE Healthcare, Menlo Park, California, USA.

[2]Department of Radiology, University of Wisconsin, Madison, Wisconsin, USA.

[3]Department of Biomedical Engineering, University of Wisconsin, Madison, Wisconsin, USA.

[4]Department of Medical Biophysics, The University of Western Ontario, London, Ontario, Canada.

[5]Department of Physics, The University of Western Ontario, London, Ontario, Canada.

[6]Department of Biomedical Engineering, The University of Western Ontario, London, Ontario, Canada.

[7]Department of Radiology, University of California, San Diego, California, USA.

[8]Applied Science Laboratory, GE Healthcare, Madison, Wisconsin, USA.

[9]Department of Medical Physics, University of Wisconsin, Madison, Wisconsin, USA.

[10]Department of Medicine, University of Wisconsin, Madison, Wisconsin, USA.

*Correspondence to: Huanzhou Yu, Ph.D., 333 Ravenswood Ave. Bldg 307, Menlo Park, California 94025. E-mail: huanzhou.yu@ge.com
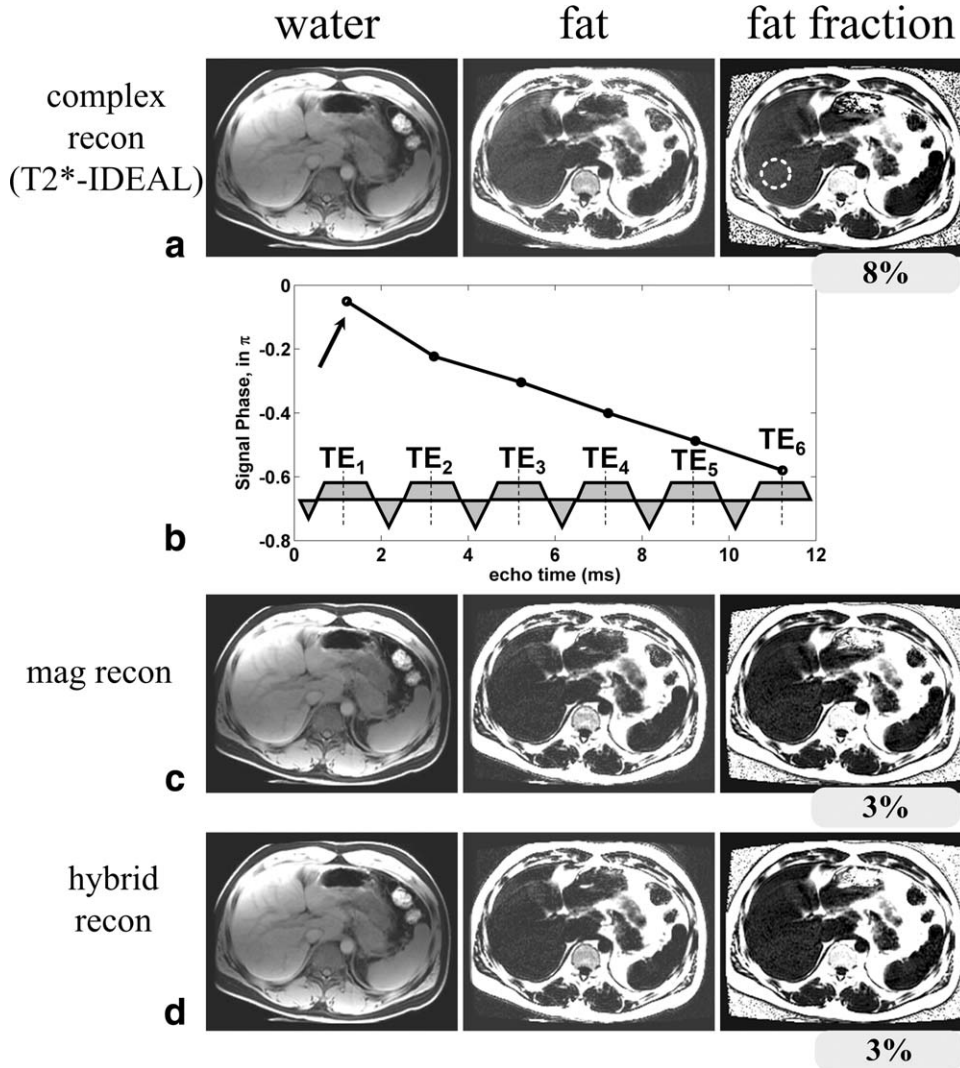
FIG. 1. Reconstruction results (water, fat, and fat-fraction images) of a six-echo abdominal scan at 1.5 T using various reconstruction approaches: complex-based T_2^*-IDEAL algorithm (**a**), the magnitude-based algorithm (**c**), and the proposed complex-based and magnitude-based hybrid algorithm (**d**). Read-out direction is right-left in this scan (horizontal). An artifactual 8% of fat is measured with T_2^*-IDEAL, due to the phase error primarily modulated on the first echo using the multiecho "fly-back" sequence (**b**). Both the magnitude-based and the hybrid reconstructions reduce the apparent fat-fraction measurement to 3%. The improvement in fat-fraction is clinically relevant considering the value dropped from the abnormal range to the normal range. Imaging parameters include: $256 \times 160 \times 16$ matrix size, field of view = 35×25 cm, 6 echoes, $TE_1 = 1.2$ ms, $\Delta TE = 2$ ms, and 25-s breath-hold.

Fat with Echo Asymmetric and Least-squares Estimation (IDEAL) processing (18), a complex-based water–fat separation method based on IDEAL algorithm (19) that corrects for both T_2^* decay and the multiple spectral peaks of fat (20). Water and fat images are further used to produce fat-fraction maps with noise-bias correction (21) to directly visualize the fat percentage in the liver. The scan was performed in a healthy volunteer. An MR spectroscopic scan (not shown) confirmed that there was no fat present in the volunteer's liver. However, the fat-fraction map (Fig. 1a) obtained from T_2^*-IDEAL showed 8% fat in liver, which can be considered abnormal according to the 5.56% cut-off found by a 2349-patient study (22). This "fatty liver" artifact can be clinically significant as it is very important to identify low fat-fraction accurately for early diagnosis and treatment of fatty liver disease. Figure 1b shows the plot of the signal phase for mean signals measured from a region of interest (ROI) (10×10 voxels) placed in liver together with the read-out gradient waveforms used in this scan. All six echoes are collected in one repetition (pulse repetition time) with a 3D multiecho SPoiled Gradient Recalled acquisition (SPGR) sequence and fly-back gradients. For a voxel containing only water, the phase of the signals should evolve linearly at a rate proportional to the B_0 field inhomogeneity. In Fig. 1b, however, the phase of the first echo (arrow) is slightly deviated from the linear curve that the last 5 echoes follow. This is due to the fact that the prewinder gradient preceding the first read-out gradient is different from the fly-back gradient preceding the read-out gradient of the other echoes. This difference causes inconsistent eddy current-generated phase modulation and results in imperfect water–fat separation that primarily varies in the read-out direction (right-left in this example).

MATERIALS AND METHODS

The flow diagram of the proposed hybrid approach is illustrated in Fig. 2. We elaborate each component in the following.

Complex-Based Water-Fat Separation Method

There are many multiecho water–fat separation methods that are based on complex source signals. In our approach, a T_2^* corrected iterative water–fat separation method (T_2^*-IDEAL) (18,19) that uses multipeak spectral modeling of fat (20) and noise bias correction (21) is used. T_1 related
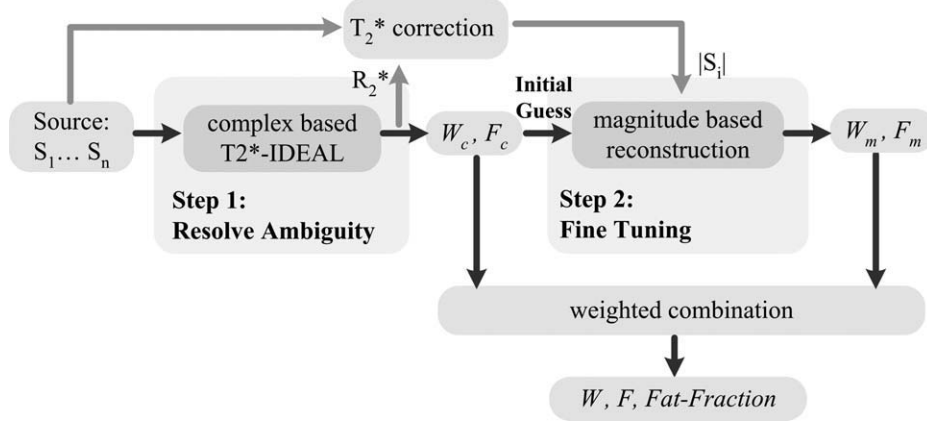
FIG. 2. Flow diagram of the proposed hybrid water-fat separation algorithm, based on a two-step approach. The first step applies complex-based T_2^*-IDEAL to reconstruct water, fat, and R_2^* maps from the multiecho complex source signals. The water and fat images are used as an initial guess for the following second step, where water–fat separation is performed using only the magnitude signals. R_2^* values from the first step are used to correct the source images, thus simplifying the fitting algorithm in the 2nd step. This two-step processing results in another set of water and fat estimates. The water and fat images from the two steps are further combined, weighted by the results from the first step, forming the final estimates of water, fat, and fat-fraction images. For simplicity, we refer to the two-step approach without weighted combination as the "magnitude-based" water–fat separation algorithm, whereas the final estimates with the weighted combination are from the "hybrid" method.

bias is avoided by using a low flip angle (21). Six echoes are collected with a multiecho 3D-SPGR sequence using fly-back gradients (Fig. 1b). The complex source data are then processed using the T_2^*-IDEAL algorithm to produce water (W_c), fat (F_c), and R_2^* maps. A region growing algorithm is applied to provide robust field map estimation and thus to resolve water–fat ambiguity (9).

Magnitude-Based Water-Fat Separation Method

The magnitude-based methods alone are unable to use the phase information to uniquely label water and fat signals. Therefore, these methods alone do not provide separated water and fat images. Figure 2 illustrates a two-step approach, in which the magnitude-based reconstruction is applied following the complex-based T_2^*-IDEAL. The results from the first step (T_2^*-IDEAL) are used as the initial guess for the magnitude-based reconstruction. The water and fat estimated from step 1 should be very close to the true water and fat quantities even in the presence of the phase errors. Therefore, they serve as an excellent initial guess for the estimation in the step 2, ensuring fast convergence and correct identification of water and fat. The second step, magnitude reconstruction, can be viewed as fine tuning the solution from the complex-based reconstruction to provide a more accurate estimate of fat-fraction. This 2-step approach that eventually leads to the results of (W_m, F_m) is referred to as the "magnitude-based" water–fat separation method.

The magnitude-based reconstruction aims to solve the following equation:

$$\begin{aligned}|S_i|^2 &= |W + F \cdot c_i|^2 \cdot e^{-2R_2^* \cdot t_i} \\ &= [W^2 + |c_i|^2 F^2 + 2 \cdot Re\{c_i\} \cdot W \cdot F] \cdot e^{-2R_2^* \cdot t_i} \\ &= [W^2 + a_i^2 \cdot F^2 + 2 \cdot b_i \cdot W \cdot F] \cdot e^{-2R_2^* \cdot t_i}\end{aligned} \quad [1]$$

where W and F are water and fat contents, i is the echo index ($i = 1, 2... $n, where n is the number of echoes). c_i

is the fat signal modulation term. For single peak modeling of the fat spectrum, c_i can be described as:

$$c_i = e^{j2\pi\Delta f\, t_i}$$

where Δf is the chemical shift between water and fat. For convenience, we have used $a_i = |c_i|$ and $b_i = Re\{c_i\}$.

Note that for the described modeling of the fat signal, $a_i = 1$. Consequently, W and F are exchangeable in Eq. 1 without altering the value of the equation. This is the inherent water–fat ambiguity, which cannot be resolved without other a priori information.

When a more accurate fat spectrum is modeled with multiple (P) spectral peaks (13,20), represented by relative amplitudes α_p and frequencies Δf_p, we have:

$$c_i = \sum_{p=1}^{P} \alpha_p e^{j2\pi\Delta f_p\, t_i}$$

In this multipeak model, $a_i = |c_i|$ is in general no longer equal to 1. Although exchanging water and fat in Eq. 1 now changes the value of the equation, the water–fat swapped solution is reflected as a local minimum when solving Eq. 1, resulting in a similar water–fat ambiguity challenge as the single peak model.

Because of the nonlinear and nonconvex nature of Eq. 1, it is often solved with iterative nonlinear data fitting algorithms. To simplify the nonlinear fitting in the magnitude-based reconstruction, the source signals are corrected for T_2^* decay using the T_2^* estimate from the complex-based T_2^*-IDEAL before the magnitude-based reconstruction, as shown in Fig. 2. This is based on the consideration that the algorithm largely relies on the magnitude changes between the echoes to estimate T_2^*, so the error in estimated T_2^* is small. In addition, T_2^* is often over-estimated using the magnitude signals if the noise bias is not taken into account (23). With T_2^*
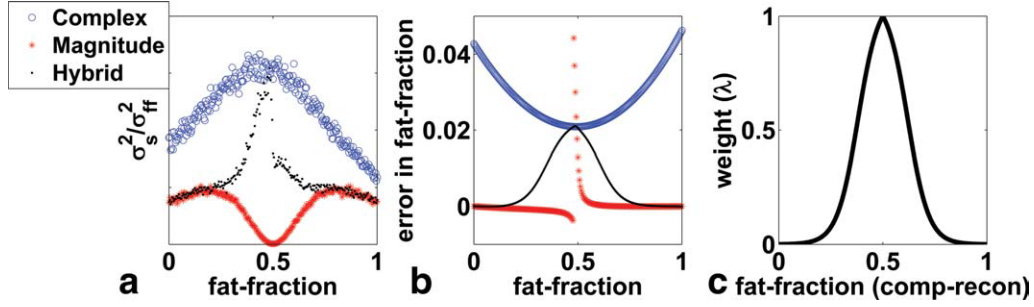
FIG. 3. Noise performance (**a**) and errors (**b**) of simulations comparing the complex (blue circle), magnitude (red star), and proposed hybrid method (black dot). σ_s and σ_{ff} denote the noise standard deviation measured in the source images and the fat-fraction images, respectively. The hybrid approach applies a Fermi weighting function (**c**) that combines the water and fat estimated with the magnitude-based and complex-based reconstructions.

estimation removed in the magnitude-based algorithm, Eq. 1 can be simplified as:

$$\left|S_i'\right|^2 = |S_i|^2 \cdot e^{2R_2^* \cdot t_i} = W^2 + a_i^2 \cdot F^2 + 2 \cdot b_i \cdot W \cdot F \quad [2]$$

A simple iterative Gauss-Newton nonlinear curve fitting (24) is then used to solve Eq. 2, as described in the Appendix.

Noise Performance Simulations

Simulations were used to study the noise performance and accuracy of the complex-based and magnitude-based reconstructions. Source signals were generated with a typical protocol [6 echoes, echo time $(TE)_1 = 1.2$ ms, $\Delta TE = 2$ ms, $R_2^* = 50$ s^{-1}] and sweeping fat-fraction from 0 to 100%. Gaussian distributed noise was added to the 6-echo source images. To simulate the effect of the eddy currents, a phase error (0.1π) was modulated on the first echo. This process was repeated 1000 times. Both complex-based water–fat separation (i.e., T_2^*-IDEAL) and the magnitude-based reconstruction described above were performed. The ratio of the noise variance in the source images (σ_s^2) and the noise variance in the resulting fat-fraction images (σ_{ff}^2) was calculated and is shown in Fig. 3a. Larger ratios indicate improved noise behavior in the separation algorithm. The magnitude-based reconstruction, implemented as the two-step approach in Fig. 2, demonstrates poor noise performance near fat-fractions close to 50%, whereas the complex-based reconstruction results in relatively better noise behavior throughout all fat-fractions, in agreement with an earlier study (18). Figure 3b shows the bias (i.e., absolute error) of the fat-fraction measured from the two reconstructions. The complex-based T_2^*-IDEAL is sensitive to phase errors on the first echo near 0% or 100% fat-fraction, as expected. The magnitude-based reconstruction is generally insensitive to the phase error except near 50% fat due to its poor noise performance in that range.

Complex-Based and Magnitude-Based "Hybrid" Approach

As shown in Figure 3a,b, the complex-based reconstruction provides relatively superior noise performance; however, the accuracy is compromised by the bias cre-

ated by the presence of phase errors, particularly at low- and high- fat-fraction. The magnitude-based reconstruction on the other hand has poor noise performance around 50%; however, it is in general more accurate in the presence of phase errors. To combine the strengths of these two approaches, we introduce a "hybrid" algorithm, in which the final water and fat images (W and F) are obtained from a weighted combination of the water and fat images from the two reconstruction steps, as illustrated in Fig. 2 (W_c and F_c from complex-based reconstruction, W_m and F_m from magnitude-based reconstruction):

$$\begin{aligned} W &= \lambda \cdot W_c + (1 - \lambda) \cdot W_m \\ F &= \lambda \cdot F_c + (1 - \lambda) \cdot F_m \end{aligned} \quad [3]$$

The weight λ is determined from the fat-fraction calculated from the first step of complex-based T_2^*-IDEAL. In our approach, a Fermi function (25) is used (Fig. 3c). When fat-fraction resulting from the complex-based reconstruction is close to 0 or 100%, λ approaches 0 such that the water and fat images from magnitude-based reconstruction are used. On the other hand, when fat-fraction from the first step is near 50%, λ approaches 1 such that the fat fraction calculated from the complex-based reconstruction contributes most to the final results.

In Fig. 3a,b, the black dotted curves represent simulation results from the hybrid approach. The noise performance is more favorable at fat-fractions near 50% than the magnitude-based method. Although a small error is introduced near 50%, low- and high-fat-fractions are more accurately estimated, which is critical for liver fat quantification. However, the improved accuracy at low fat-fractions is at the cost of reduced noise performance in those ranges compared with the complex reconstruction.

Experiments

In vivo scanning was performed on GE 1.5 T and 3 T scanners (HDx, GE Healthcare, Waukesha, WI) to evaluate the various approaches described. Informed consent and permission from our Institutional Review Board were obtained. A 3D-SPGR multiecho sequence was used to collect six echoes with "fly-back" gradients. For each

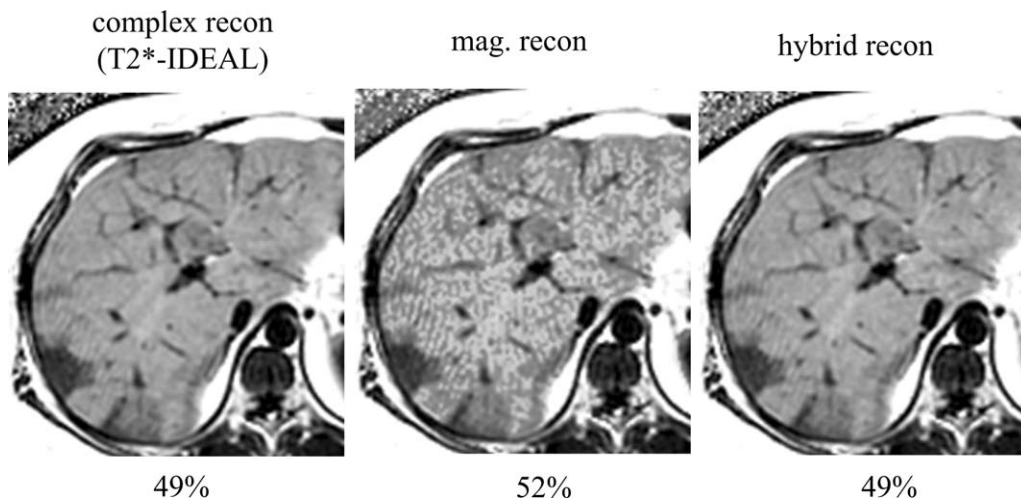complex recon (T2*-IDEAL) — 49%   mag. recon — 52%   hybrid recon — 49%

FIG. 4. Results from a six-echo scan at 3 T in a patient with significant fatty infiltration of liver. Fat-fraction images of various approaches are shown. Images are cropped to the liver area of interest. The fat-fraction is 49% measured from complex-based T_2^*-IDEAL. As predicted by the simulations, the magnitude-based reconstruction demonstrates noisy fat-fraction estimated in liver, which is not present in the fat-fraction image produced by the hybrid reconstruction due to the weighted combination process. Imaging parameters include: 192 × 192 × 16 matrix size, field of view = 44 × 33 cm, 6 echoes interleaved in 2 repetitions, TE_1 = 0.8 ms, ΔTE = 0.7 ms, and 26-s breath-hold.

scan, water–fat separation was performed using complex-based (T_2^*-IDEAL), the magnitude-based, and the hybrid methods using the same source data. The fat-fraction images were generated from the separated water and fat images and evaluated for each approach.

Comparison With MR Spectroscopy

To demonstrate that the hybrid reconstruction improves the accuracy of the fat-fraction measurements, comparison of MRI measured fat-fraction with MR spectroscopy measured fat-fraction was made in 58 studies (55 patients with 3 patients scanned twice) at 1.5 T that do not include the in vivo scans mentioned earlier. All studies were performed with Institutional Review Board approval and informed written consent. As a reference standard, single voxel magnetic resonance spectroscopy (MRS) using stimulated echo acquisition mode was performed (26). Imaging parameters of MRI include: 256 × 128 × 24 matrix size, field of view = 35 × 35 cm, 6 echoes, TE_1 = 1.3 ms, ΔTE = 2.0 ms, 5 degree flip angle, and 21-second breath-hold with parallel imaging acceleration. Imaging parameters of MRS included: voxel size = 20 × 20 × 25 mm^3, pulse repetition time = 3.5 s to minimize T_1 weighting, 2048 readout points, 1 signal average, receiver bandwidth = ±5 kHz, and 5 echo times at 10, 20, 30, 40, 50 ms (to facilitate T_2 correction), requiring a 21 s breath-hold. The MRS voxel was placed in the right hepatic lobe avoiding large blood vessels and other non-liver tissues. All MRS data were postprocessed by an MR physicist blinded to the MRI results, using AMARES algorithm (27) in jMRUI (28). The comparison between MRS and imaging results using the hybrid reconstruction will also be included in a separate clinical study (29) based on an earlier report (30). In this work, we retrospectively reconstructed the imaging data of all patients using the complex-based T_2^*-IDEAL as well as the hybrid method. Fat-fraction measurements were obtained in

ROIs drawn in the liver co-localized with the MRS voxel and perfectly co-registered between the two reconstructions and were compared with the MR spectroscopy measured fat-fraction.

RESULTS

Figure 1 shows results from a healthy volunteer at 1.5 T, reconstructed by the complex-based T_2^*-IDEAL, the magnitude-based reconstruction, and the hybrid approach, respectively. The complex-based T_2^*-IDEAL results in 8% of artifactual fat in liver, whereas spectroscopy (not shown) confirms no presence of fat in liver. With the magnitude-based reconstruction and the hybrid approach, the fat-fraction measured in liver is reduced to 3%. This improvement may be clinically significant as the diagnosis of steatosis is typically made when liver fat content exceeds 5.56% (22). Additionally, the magnitude and the hybrid reconstructions successfully produced separated water and fat images with the help of the results from the complex reconstruction in the first step.

Results from a patient with severe steatosis at 3 T are presented in Fig. 4. The complex-based reconstruction measures 49% fat in liver. As predicted by simulations shown in Fig. 3, the magnitude-based reconstruction leads to substantial noisy artifact in the liver due to its poor noise performance near 50%. This artifact is removed in the hybrid approach, where the weighted combination of the liver fat-fraction measurements is dominated by the results of the complex reconstruction.

In 58 patient scans at 1.5 T, the MRI measured fat-fraction is compared with the MRS measured fat-fraction. The in vivo scans shown in Figs. 1 and 4 were not part of this study. The correlation and Bland–Altman plots are shown in Fig. 5. The complex-based T_2^*-IDEAL results in fat-fraction bias at the low fat-fraction regime, which results in a slope of 0.91 and intercept of 2.17%.
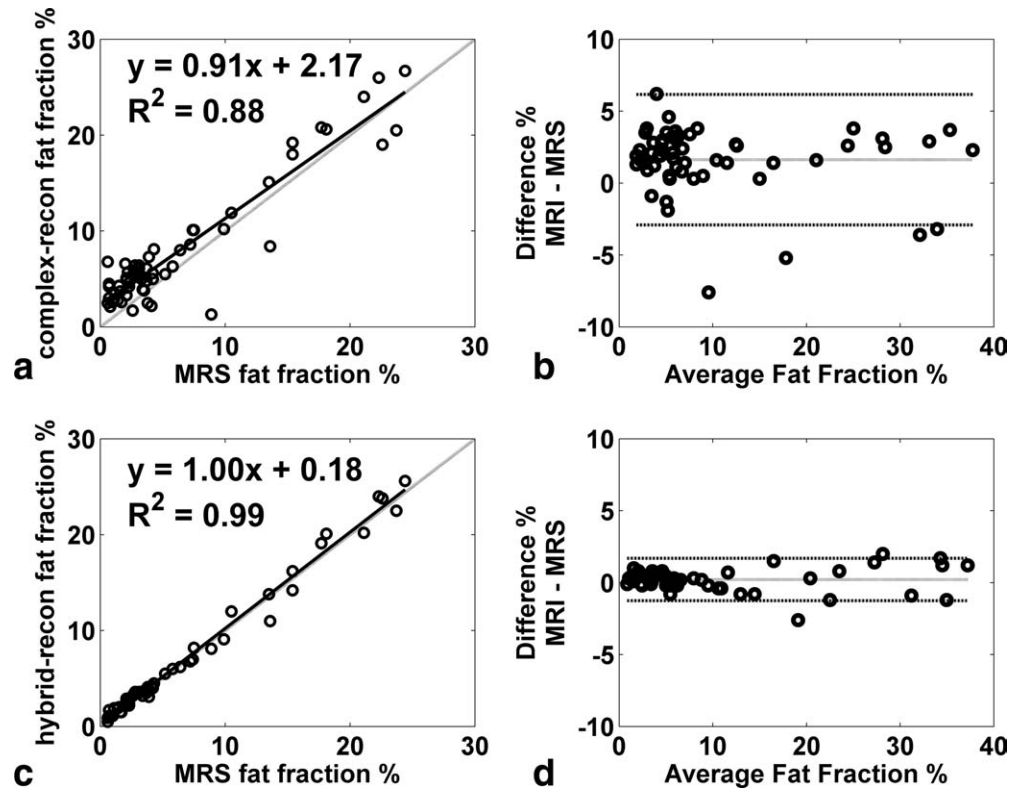
FIG. 5. Comparison of MR spectroscopy measured fat-fraction with imaging measured fat-fraction in 58 studies in the format of correlation plot and Bland–Altman plot. With complex-based T_2^*-IDEAL reconstruction (**a**), substantial bias is seen with the low fat-fraction measurement. From the Bland–Altman plot (**b**), the mean of the difference is 1.6% and the 95% confidence interval is (−2.9%, 6.2%). The correlation is improved with the hybrid reconstruction (**c**), particularly at low fat fraction regime, which is also reflected in the tighter Bland–Altman plot (**d**) [mean of the difference: 0.2%, 95% confidence interval: (−1.3%, 1.7%)]. In (a) and (c), the solid lines represent linear regression, whereas the dashed line denotes the identity line ($Y = X$).

With the hybrid reconstruction, the agreement between MRS and MRI is substantially improved (slope = 1.00, intercept = 0.18%), demonstrating the importance of correcting phase errors for quantitative fat imaging applications. The improvement can also be seen from the Bland–Altman plots, where the hybrid reconstruction leads to a much tighter 95% confidence interval [(−1.3%, 1.7%) vs. (−2.9%, 6.2%)] from complex-based reconstruction). The sensitivity and specificity of the complex-based reconstruction are 0.95 (18/19) and 0.69 (27/39), respectively, compared with 1 (19/19) and 1 (39/39) from the new hybrid reconstruction. Note that the correlation as well as sensitivity and specificity of the hybrid reconstruction were also included in the results of Meisamy et al. (29). The limitation of the study is that no patient was found to possess fat-fraction higher than 30%. In addition, the magnitude-only reconstruction was not performed. The performance of the magnitude-only reconstruction is expected to be similar to the hybrid reconstruction as none of the patients included in this study has fat-fraction near 50%.

DISCUSSION

Conventional multipoint chemical shift water–fat separation methods rely heavily on phase information to separate water and fat. As a result, they are sensitive to phase errors, such as those from eddy currents. For quantitative applications, we have shown that the phase errors can lead to a clinically relevant bias particularly at low fat-fractions. The challenge of accurate low fat-fraction measurement has also been observed in other studies using chemical shift based water–fat separation methods (4,31,32). Considering that one study concluded the cut-off fat-fraction for normal vs. abnormal liver is ∼5.56% (22), a clinically useful fat quantification technique must be capable of quantifying fat accurately, particularly at low fat-fractions.

In this work, we introduced a hybrid multipoint water–fat separation approach, where a T_2^*-corrected, spectrally modeled "complex based" water–fat separation method (T_2^*-IDEAL) is followed by a fitting algorithm based on magnitude multiecho signals. The results from the two steps are combined for the final estimate of water and fat to remove the effects of phase errors as well as to avoid poor noise performance at fat-fractions near 50%. The second step, based on magnitude signals, relies on the results from the first step for initial conditioning of the fit to achieve a full dynamic range from 0 to 100%.

As T_2^* decay contains no phase information, we have assumed that the T_2^* estimated from the complex water–fat separation is sufficiently accurate and can be used to correct the source signals, such that additional T_2^* correction is not required in step 2. This approximation allows

much simpler nonlinear fitting because no exponential terms ($e^{-\text{TE}/T_2^*}$) are involved. In addition, the complex method provides a relatively accurate (although not perfect) initial estimate of water and fat signals, and therefore, the magnitude-based fitting is very fast, typically requiring only a few iterations for convergence. Therefore, minimal additional computational overhead is necessary for the hybrid approach compared with the complex-based method.

Despite better accuracy, our two-step implementation of the magnitude-based reconstruction has poor noise performance near 50%, which is likely a manifestation of water–fat ambiguity. For those magnitude-based reconstruction methods that only attempt to estimate fat-fraction in a 50% dynamic range (13), it is possible that they do not suffer from this noise problem near 50%. To alleviate this noise performance limitation, a weighted combination of the results from the two reconstructions was proposed. This combination weights the contribution from the magnitude-based reconstruction more heavily at low fat-fractions and the complex-based reconstruction is weighted more heavily near 50%. In our work, we chose a Fermi function to achieve smooth transition between the two regimes. However, there are many weighting functions that could be chosen to achieve the same goals. Despite the weighted combination, the improved accuracy at the low fat fractions with the hybrid reconstruction is at the cost of reduced noise performance compared with the complex-reconstruction.

The phase errors from eddy currents could also be removed with alternative methods. For example, if the phase errors were always in the first echo, it is possible to formulate a problem that fits the model using only the magnitude of the first echo signal in addition to complex signals of the rest 5 echoes. Another approach would be to perform an estimate from the last five echoes first, the results of which are used to extrapolate a phase for the first echo, replacing the initial erroneous phase. A six-echo T_2^*-IDEAL can then be performed. However, it is not ideal to discard the first echo as the first echo has the best SNR in methods that model T_2^* (18). The hybrid approach we proposed in this work can also be used for removing more general phase errors, for example, phase errors in water–fat separation methods with bipolar gradients (non-fly-back) (33,34).

In conclusion, the proposed complex-based and magnitude-based hybrid water–fat separation method is an effective approach for removing undesired phase errors for fat-fraction measurement. Correction of unwanted phase shifts leads to significantly improved accuracy for quantification of low fat-fractions, which may be the most clinically relevant for methods used for screening and diagnosis of hepatic steatosis.

ACKNOWLEDGMENTS

APPENDIX

We describe a simple iterative nonlinear fitting algorithm to solve Eq. 2, which is shown in the following (Eq. A1) for convenience.

$$\left|S_i'\right|^2 = \left|S_i\right|^2 \cdot e^{2R_2^* \cdot t_i} = W^2 + a_i^2 \cdot F^2 + 2 \cdot b_i \cdot W \cdot F \qquad [\text{A1}]$$

Step 1: Use initial estimates of water and fat based on those from the complex-based T_2^*-IDEAL (W_c, F_c) water–fat separation, i.e.:

$$\hat{W} = W_\text{c}, \quad \hat{F} = F_\text{c}$$

Step 2: Calculate the signals corresponding to the current estimates:

$$\left|S_i'\right|^2 = \hat{W}^2 + a_i^2 \cdot \hat{F}^2 + 2 \cdot b_i \cdot \hat{W} \cdot \hat{F}$$

Step 3: Calculate the error terms:

$$
\begin{aligned}
\left|S_i'\right|^2 - \left|\hat{S}_i'\right|^2 &= 2 \cdot \hat{W} \cdot \Delta W + 2 \cdot a_i^2 \cdot \hat{F} \cdot \Delta F + 2 \cdot b_i \cdot \hat{W} \cdot \Delta F \\
&\quad + 2 \cdot b_i \cdot \hat{F} \cdot \Delta W \\
&= (2 \cdot \hat{W} + 2 \cdot b_i \cdot \hat{F}) \cdot \Delta W \\
&\quad + (2a_i^2 \cdot \hat{F} + 2 \cdot b_i \cdot \hat{W}) \cdot \Delta F
\end{aligned}
$$

We now define the matrix **B** as:

$$
\mathbf{B} = \begin{bmatrix}
2 \cdot \hat{W} + 2 \cdot b_1 \cdot \hat{F} & 2 \cdot a_1^2 \cdot \hat{F} + 2 \cdot b_1 \cdot \hat{W} \\
2 \cdot \hat{W} + 2 \cdot b_2 \cdot \hat{F} & 2 \cdot a_2^2 \cdot \hat{F} + 2 \cdot b_2 \cdot \hat{W} \\
\cdots & \cdots \\
2 \cdot \hat{W} + 2 \cdot b_\text{nte} \cdot \hat{F} & 2 \cdot a_\text{nte}^2 \cdot \hat{F} + 2 \cdot b_\text{nte} \cdot \hat{W}
\end{bmatrix}
$$

Therefore, a linear least squares inversion will give an estimate of the error terms (ΔW and ΔF):

$$
\begin{bmatrix} \Delta W \\ \Delta F \end{bmatrix} = (\mathbf{B}^T \cdot \mathbf{B})^{-1} \cdot \mathbf{B}^T \cdot
\begin{bmatrix}
\left|S_1'\right|^2 - \left|\hat{S}_1'\right|^2 \\
\left|S_2'\right|^2 - \left|\hat{S}_2'\right|^2 \\
\cdots \\
\left|S_\text{nte}'\right|^2 - \left|\hat{S}_\text{nte}'\right|^2
\end{bmatrix}
$$

Step 4: Update the current estimates

$$\hat{W} := \hat{W} + \Delta W, \quad \hat{F} := \hat{F} + \Delta F$$

Step 5: Go to step 2, unless iteration converges or the maximum number of iteration is reached.

REFERENCES

1. Ma J. Dixon techniques for water and fat imaging. J Magn Reson Imaging 2008;28:543–558.
2. Bley TA, Wieben O, Francois CJ, Brittain JH, Reeder SB. Fat and water magnetic resonance imaging. J Magn Reson Imaging 2010;31:4–18.
3. Hussain HK, Chenevert TL, Londy FJ, Gulani V, Swanson SD, McKenna BJ, Appelman HD, Adusumilli S, Greenson JK, Conjeevaram HS. Hepatic fat fraction: MR imaging for quantitative measurement and display—early experience. Radiology 2005;237:1048–1055.
4. Kim H, Taksali SE, Dufour S, Befroy D, Goodman TR, Petersen KF, Shulman GI, Caprio S, Constable RT. Comparative MR study of hepatic fat quantification using single-voxel proton spectroscopy, two-point dixon and three-point IDEAL. Magn Reson Med 2008;59:521–527.
5. Reeder SB, Robson PM, Yu H, Shimakawa A, Hines CD, McKenzie CA, Brittain JH. Quantification of hepatic steatosis with MRI: the effects of accurate fat spectral modeling. J Magn Reson Imaging 2009; 29:1332–1339.
6. Maas M, Hollak CE, Akkerman EM, Aerts JM, Stoker J, Den Heeten GJ. Quantification of skeletal involvement in adults with type I

Gaucher's disease: fat fraction measured by Dixon quantitative chemical shift imaging as a valid parameter. AJR Am J Roentgenol 2002; 179:961–965.

7. Xiang QS, An L. Water-fat imaging with direct phase encoding. J Magn Reson Imaging 1997;7:1002–1015.

8. Ma J. Breath-hold water and fat imaging using a dual-echo two-point Dixon technique with an efficient and robust phase-correction algorithm. Magn Reson Med 2004;52:415–419.

9. Yu H, Reeder SB, Shimakawa A, Brittain JH, Pelc NJ. Field map estimation with a region growing scheme for iterative 3-point water-fat decomposition. Magn Reson Med 2005;54:1032–1039.

10. Lu W, Hargreaves BA. Multiresolution field map estimation using golden section search for water-fat separation. Magn Reson Med 2008;60:236–244.

11. Hernando D, Kellman P, Haldar JP, Liang ZP. Robust water/fat separation in the presence of large field inhomogeneities using a graph cut algorithm. Magn Reson Med 2010;63:79–90.

12. Ford JC, Wehrli FW. In vivo quantitative characterization of trabecular bone by NMR interferometry and localized proton spectroscopy. Magn Reson Med 1991;17:543–551.

13. Bydder M, Yokoo T, Hamilton G, Middleton MS, Chavez AD, Schwimmer JB, Lavine JE, Sirlin CB. Relaxation effects in the quantification of fat using gradient echo imaging. Magn Reson Imaging 2008;26:347–359.

14. Dixon WT. Simple proton spectroscopic imaging. Radiology 1984; 153:189–194.

15. Chang JS, Taouli B, Salibi N, Hecht EM, Chin DG, Lee VS. Opposed-phase MRI for fat quantification in fat-water phantoms with 1H MR spectroscopy to resolve ambiguity of fat or water dominance. AJR Am J Roentgenol 2006;187:W103–W106.

16. Hollingsworth KG, Abubacker MZ, Joubert I, Allison ME, Lomas DJ. Low-carbohydrate diet induced reduction of hepatic lipid content observed with a rapid non-invasive MRI technique. Br J Radiol 2006;79:712–715.

17. O'Regan DP, Callaghan MF, Wylezinska-Arridge M, Fitzpatrick J, Naoumova RP, Hajnal JV, Schmitz SA. Liver fat content and T_2^*: simultaneous measurement by using breath-hold multiecho MR imaging at 3.0 T—feasibility. Radiology 2008;247:550–557.

18. Yu H, McKenzie CA, Shimakawa A, Vu AT, Brau AC, Beatty PJ, Pineda AR, Brittain JH, Reeder SB. Multiecho reconstruction for simultaneous water-fat decomposition and T_2^* estimation. J Magn Reson Imaging 2007;26:1153–1161.

19. Reeder SB, Wen Z, Yu H, Pineda AR, Gold GE, Markl M, Pelc NJ. Multicoil Dixon chemical species separation with an iterative least-squares estimation method. Magn Reson Med 2004;51:35–45.

20. Yu H, Shimakawa A, McKenzie CA, Brodsky E, Brittain JH, Reeder SB. Multiecho water-fat separation and simultaneous R_2^* estimation with multifrequency fat spectrum modeling. Magn Reson Med 2008; 60:1122–1134.

21. Liu CY, McKenzie CA, Yu H, Brittain JH, Reeder SB. Fat quantification with IDEAL gradient echo imaging: correction of bias from T(1) and noise. Magn Reson Med 2007;58:354–364.

22. Szczepaniak LS, Nurenberg P, Leonard D, Browning JD, Reingold JS, Grundy S, Hobbs HH, Dobbins RL. Magnetic resonance spectroscopy to measure hepatic triglyceride content: prevalence of hepatic steatosis in the general population. Am J Physiol Endocrinol Metab 2005; 288:E462–E468.

23. Positano V, Salani B, Pepe A, Santarelli MF, De Marchi D, Ramazzotti A, Favilli B, Cracolici E, Midiri M, Cianciulli P, Lombardi M, Landini L. Improved T_2^* assessment in liver iron overload by magnetic resonance imaging. Magn Reson Imaging 2009;27:188–197.

24. Nash S, Sofer A. Linear and nonlinear programming. New York: The McGraw-Hill Companies, Inc.; 1996.

25. Bernstein MA, King KF, Zhou XJ. Handbook of MRI pulse sequences. Boston: Elsevier; 2004.

26. Hamilton G, Middleton MS, Bydder M, Yokoo T, Schwimmer JB, Kono Y, Patton HM, Lavine JE, Sirlin CB. Effect of PRESS and STEAM sequences on magnetic resonance spectroscopic liver fat quantification. J Magn Reson Imaging 2009;30:145–152.

27. Vanhamme L, van den Boogaart A, Van Huffel S. Improved method for accurate and efficient quantification of MRS data with use of prior knowledge. J Magn Reson 1997;129:35–43.

28. Naressi A, Couturier C, Devos JM, Janssen M, Mangeat C, de Beer R, Graveron-Demilly D. Java-based graphical user interface for the MRUI quantitation package. MAGMA 2001;12:141–152.

29. Meisamy S, Hines C, Hamilton G, Sirlin C, McKenzie C, Yu H, Brittain JH, Reeder S. Quantification of hepatic steatosis using T_1 independent, T_2^* corrected MRI with spectral modeling of fat: a blinded comparison with MR spectroscopy. Radiology 2011 [Epub ahead of print].

30. Meisamy S, Hines C, Hamilton G, Vigen K, Brittain J, McKenzie C, Yu H, Nagle S, Zeng Y, Sirlin C, Reeder S. Validation of chemical shift based fat-fraction imaging with MR spectroscopy. In: Proceedings 17th Scientific Meeting, International Society for Magnetic Resonance in Medicine, HI, USA; 2009. p 207.

31. Borra R, Nuutila P, Parkkola R, Komu M, Lautamäki R, Salo S, Dean K. Rapid evaluation of liver fat content using in-out-phase imaging in nonalcoholic fatty liver disease. In: Proceedings 16th Scientific Meeting, International Society for Magnetic Resonance in Medicine, Honolulu, HI, USA; 2008. p 3711.

32. Irwan R, Edens M, Sijens P. Overestimation of liver fat content in fast Dixon-based MRI method compared with multi-voxel MR spectroscopy quantification. In: Proceedings 16th Scientific Meeting, International Society for Magnetic Resonance in Medicine, Toronto, Canada; 2008. p 3710.

33. Lu W, Yu H, Shimakawa A, Alley M, Reeder SB, Hargreaves BA. Water-fat separation with bipolar multiecho sequences. Magn Reson Med 2008;60:198–209.

34. Eggers H, Koken P, Boernert P. Phase and amplitude correction in bipolar multi-gradient-echo water-fat imaging. In: Proceedings 16th Scientific Meeting, International Society for Magnetic Resonance in Medicine, Toronto, Canada; 2008. p 1364.